Traitement du Signal
Vol. 41, No. 5, October, 2024, pp. 2317-2326
Journal homepage: http://iieta.org/journals/ts

Application of Multispectral and Thermal Imaging Technologies in Drone Search and Rescue Missions

Jie Xu

Investigation College, Nanjing Police University, Nanjing 210023, China

Corresponding Author Email: 114104@njpu.edu.cn

https://doi.org/10.18280/ts.410508

Received: 11 April 2024
Revised: 26 August 2024
Accepted: 10 September 2024
Available online: 31 October 2024

Keywords:
drone, search and rescue, multispectral, thermal imaging, temperature distribution model, temperature inversion, multi-temporal detection

ABSTRACT

With the rapid development of drone technology, its application in search and rescue missions is becoming increasingly widespread. Traditional rescue methods, constrained by manpower and ground equipment, exhibit numerous shortcomings in efficiency and applicability. Multispectral and thermal imaging technologies have emerged as crucial auxiliary tools for drones, capable of operating effectively in complex environments and varying light conditions. These technologies leverage spectral information across different bands and thermal radiation characteristics to significantly enhance target recognition and localization accuracy. However, existing research primarily focuses on single-band image processing and basic thermal data handling, revealing considerable limitations in complex environments and a lack of in-depth studies on establishing and solving target temperature distribution models. This paper aims to develop a temperature distribution model for search and rescue targets using drones, propose and solve the model, and further explore multispectral temperature inversion and multi-temporal detection methods. The goal is to improve the accuracy and efficiency of rescue missions, providing new technological support and theoretical foundations for the application of drones in public safety and emergency management.

1. INTRODUCTION

In recent years, with the rapid development of drone technology and its widespread application in various tasks, the role of drones in search and rescue missions has become increasingly prominent [1-4]. Traditional search and rescue tasks primarily rely on manpower and ground equipment, which not only results in low efficiency but also poses numerous limitations in complex environments [5, 6]. Multispectral and thermal imaging technologies offer new possibilities for drone applications in search and rescue due to their ability to penetrate smoke, dust, and operate under various lighting conditions [7-9]. These technologies capture spectral information across different bands and the thermal radiation characteristics of target objects, enabling more accurate identification and localization of missing persons and trapped targets, thereby providing essential technical support for modern rescue operations.

Research on the application of multispectral and thermal imaging technologies in drone search and rescue tasks holds significant practical importance. Firstly, these technologies can significantly enhance rescue efficiency, shorten search and rescue times, and thereby increase the survival rates of trapped individuals [10-13]. Secondly, they can function in complex terrains and harsh weather conditions, addressing the shortcomings of traditional rescue methods. Finally, with the proliferation of drones and the maturation of technology, related research will further promote the use of drones in public safety and emergency management, providing strong support for social stability and disaster response [9, 14-16].

Despite the enormous potential of multispectral and thermal imaging technologies in drone rescue operations, existing research methods still have many shortcomings. Currently, most studies focus on single-band image processing and have not fully explored the advantages of multispectral information [17, 18]. Furthermore, many methods for processing thermal imaging data and target identification rely on simple threshold segmentation or traditional image processing algorithms, making it difficult to cope with noise interference and false target issues in complex environments [19-21]. Existing research on establishing and solving target temperature distribution models is also relatively crude, lacking in-depth consideration of actual application scenarios.

The aim of this study is to address these shortcomings by establishing and solving a temperature distribution model for drone search and rescue targets, thereby enhancing the accuracy and reliability of multispectral temperature inversion and multi-temporal detection. Specifically, this paper consists of three main parts: first, establishing a temperature distribution model for drone search and rescue targets to accurately describe the temperature variation characteristics of targets under different environmental conditions; second, proposing and solving this temperature distribution model to improve the accuracy of target identification and localization; and finally, researching multispectral temperature inversion and multi-temporal detection methods to enhance detection

performance and stability in complex environments. Through these studies, this paper will provide new technical means and theoretical support for the application of drones in search and rescue missions, holding significant academic and practical application value.

2. ESTABLISHMENT OF THE TEMPERATURE DISTRIBUTION MODEL FOR DRONE SEARCH AND RESCUE TARGETS

To establish a thermal model for detecting search and rescue targets using infrared imaging, a series of reasonable assumptions must be made to ensure the model's feasibility and accuracy. These assumptions include:

(1) Regarding environmental conditions, it is assumed that the meteorological and geographical environment of the search and rescue area remains relatively stable. Specifically, it is assumed that during the search and rescue process, external conditions such as environmental temperature, humidity, and wind speed do not undergo drastic changes over a short period.

(2) Concerning target characteristics, it is assumed that the targets being searched for and rescued (such as missing persons or trapped individuals) possess relatively constant physiological characteristics. It is assumed that the surface temperature of the target fluctuates within a certain range and that these temperature changes can be described using known physiological models.

(3) Regarding sensor characteristics, it is assumed that the multispectral and thermal imaging sensors mounted on the drone have sufficient sensitivity and resolution to accurately capture the thermal radiation characteristics of the target. Specifically, it is assumed that the sensor's noise level is within an acceptable range and that its response time is fast enough to capture real-time temperature changes of the target.

In the thermal model of the drone search and rescue target and its surrounding area, the thermal diffusivity and thermal conductivity are the most critical thermal physical parameters. The thermal diffusivity β_0 and β_t describe the rate of heat diffusion in the target region Ψ_1 and the background region $\Psi\backslash\Psi_1$. Typically, $\beta_0>\beta_t$ because the target generally has a higher thermal diffusivity. The lower thermal diffusivity of the background region helps to more distinctly differentiate the target from the background in thermal imaging. The thermal conductivity coefficients j_0 and j_t describe the heat conduction capability of the target and background regions. The thermal conductivity coefficient j_0 of the target region may be high because objects such as the human body typically have high thermal conductivity. Conversely, the thermal conductivity coefficient j_t of the background region is lower, allowing for different thermal response characteristics in the temperature field. Specifically, let the entire region be $\Psi=\{a:0<a_u<m_u, u=1, 2, 3\}$, where the lengths of the edges along directions a_1, a_2, and a_3 are m_1, m_2, and m_3, respectively. The position of any point within the region is represented by $a=(a_1, a_2, a_3)$. The upper surface position of the target object is ϑ_1, and the lower surface position is ϑ_2. The observation time interval is $(0, s_r)$, and the temperature distribution at any point in the region is represented by $S(a, s)$.

The heat conduction equation is the fundamental equation describing how heat diffuses within an object and its surface. For the thermal model of drone search and rescue targets and their surrounding area, it is first necessary to consider the thermal physical properties of different materials and environmental media, such as thermal conductivity, specific heat capacity, and density. These properties determine how heat is transferred within the target and the environment. The heat conduction equation, based on these properties, can describe the changes in the temperature field over time and space. Through the heat conduction equation, it can be shown that $S(a, s)$ satisfies the partial differential equation given by:

$$\frac{\partial S(a,s)}{\partial s}=\beta_0\sum_{u=1}^{3}\frac{\partial^2 S(a,s)}{\partial a_u^2},(a,s)\in\Psi_1\times(0,s_r) \tag{1}$$

$$\frac{\partial S(a,s)}{\partial s}=\beta_t\sum_{u=1}^{3}\frac{\partial^2 S(a,s)}{\partial a_u^2},(a,s)\in(\Psi\setminus\Psi_1)\times(0,s_r) \tag{2}$$

Assuming the unit normal vector along the directions a_1, a_2, or a_3 is represented by v, the temperature distribution at the interface between the drone search and rescue target and the surrounding area exhibits continuity, leading to the following two boundary conditions:

$$\lim_{b\in\Psi_1,b\to a}S(b,s)=\lim_{b\in\Psi/\Psi_1,b\to a}S(b,s) \tag{3}$$

$$j_0\frac{\partial S|_{\Psi_1}}{\partial v}(a,s)=j_t\frac{\partial S|_{\Psi_1\backslash\Psi}}{\partial v}(a,s) \tag{4}$$

In drone search and rescue missions, establishing the initial conditions for the thermal model is a crucial step, as these initial conditions directly impact the accuracy of the entire model and the reliability of subsequent calculations.

The initial conditions need to describe the temperature distribution of the target and its surrounding environment at the starting observation time. In practice, the temperature distribution near the target cannot be directly obtained, necessitating the use of data acquired through multispectral and thermal imaging technologies. Thermal imaging technology can provide the temperature distribution on the surface of the target, with this data typically obtained by converting the infrared radiation intensity captured by infrared sensors. Multispectral imaging technology, on the other hand, captures spectral data across different bands to provide the thermal response characteristics of the target and its surrounding materials. Specifically, at the starting observation time, the thermal imaging equipment carried by the drone scans the search area to acquire the surface temperature distribution of the target and its surrounding region. This temperature data is recorded in the form of a two-dimensional image, denoted as $S(a, b, 0)$, where a and b represent spatial coordinates, and 0 denotes the starting time point. Assuming the temperature distribution in the vicinity of the drone search and rescue target is known, we have:

$$S(a,0)=h(a),a\in\Psi \tag{5}$$

To obtain the temperature distribution at different depths within the region, data captured from different spectral bands using multispectral imaging technology can be utilized. Figure 1 illustrates a schematic of a multispectral image. Figure 2 shows the suppression filter set used to process the background region. The processed data provides the thermal response characteristics of the target's various materials at different

depths. By analyzing this multispectral data and combining it with known thermal physical properties of the materials, it is possible to infer temperature information at certain depths based on the surface temperature distribution of the target. For temperature distributions at depths that cannot be directly measured, interpolation methods can be employed. Specifically, surface temperature distribution can be obtained from thermal imaging data, and then interpolation can be performed using multispectral data and the thermal physical properties of the materials to estimate the temperature distributions at different depths in the target and its surrounding area, denoted as $S(a, b, c, 0)$, where c represents depth.

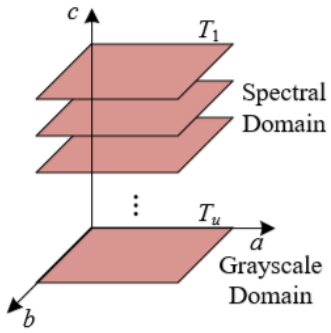

Figure 1. Schematic of multispectral image

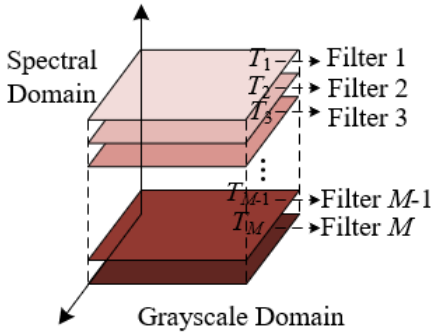

Figure 2. Suppression filter set for background region

The solution to the constructed thermal model relies on boundary conditions for surface heat exchange, which mainly include thermal radiation, thermal convection, and thermal conduction. Each of these boundary conditions is closely related to the environmental characteristics of the target area and directly impacts the analysis of sensor data and thermal imaging from the drone. Among these, the thermal radiation boundary condition is an important pathway for heat exchange between the surface and the external environment. When setting this boundary condition, factors such as solar radiation, atmospheric radiation, and surface radiation must be considered. The intensity of solar radiation varies with observation time, location, and weather conditions and can typically be obtained through meteorological data or calculated using standard models. The angle of solar incidence is also a crucial factor, as it directly affects the actual amount of radiation reaching the surface. Furthermore, atmospheric downwelling radiation depends on atmospheric conditions such as cloud cover and water vapor content, which can be determined using atmospheric radiation models or field data. Surface radiation requires consideration of surface emissivity, which differs among various materials. The thermal convection boundary condition involves heat exchange between the surface of the region and the surrounding air, primarily influenced by air movement. When setting the thermal convection boundary condition, factors such as air temperature, humidity, wind speed, and wind direction must be considered. Air temperature and humidity directly affect the intensity of thermal convection, typically provided by meteorological data or field measurements. Higher wind speeds result in a greater convective heat transfer coefficient, leading to stronger heat exchange, with wind speed and direction measurable through meteorological stations or drone sensors. The thermal conduction boundary condition involves heat transfer between the surface and subsurface. In establishing this boundary condition, the thermal conductivity, specific heat capacity, and density of surface materials, as well as the underground temperature gradient, must be considered. Let the outward normal direction at some boundary surface be represented by v, and let the solar and sky radiation absorbed by the area surrounding the drone search and rescue target be represented by w_{SU} and w_{SK}, respectively. The heat absorbed between the surface of the area and the air through thermal convection is represented by w_{CO}, and the heat radiated away from the area surrounding the drone search and rescue target is represented by w_{EM}. The boundary conditions for these heat exchanges can be set and adjusted as follows:

$$j\frac{\partial S}{\partial v}\bigg|_{Boundary\ Surface} = w_{SU} + w_{SK} + w_{CO} - w_{EM} \tag{6}$$

The surface heat exchange in the model satisfies:

$$\begin{aligned} -j_t \frac{\partial S}{\partial a_3}(a,s) &= w_{SU}(s) + w_{SK}(s) \\ +w_{CO}(a,s) &- w_{EM}(a,s) \end{aligned} \tag{7}$$

The Stefan-Boltzmann law must be satisfied:

$$\begin{aligned} &w_{EM}(a,s) = \gamma_{SO}\delta S^4(a,s), \\ &(a,s) \in \Delta_3^1 \times (0, s_r) \end{aligned} \tag{8}$$

Assuming that the weather conditions and the thermal characteristics of the area surrounding the drone search and rescue target are represented by o and $w(s)$, the above two equations can be combined to yield:

$$\begin{aligned} &-\beta_t \frac{\partial S(a,s)}{\partial a_3}(a,s) + oS(a,s) \\ &= w(s), (a,s) \in \Delta_3^1 \times (0, s_r) \end{aligned} \tag{9}$$

Assuming that the atmospheric temperature is represented by S_{AI}, the temperature distribution of the surface surrounding the drone search and rescue target is denoted by S_0, and the convective heat transfer coefficient between the area surrounding the drone search and rescue target and the atmosphere is represented by g_{CO}, the expressions for o and $w(s)$ can be given as:

$$o = \frac{\beta_t}{j_t}\left(4\gamma_{SO}\delta S_0^3 + g_{CO}\right) \tag{10}$$

$$w(s)=\frac{\beta_t}{j_t}\begin{bmatrix} w_{SU}(s)+w_{SK}(s) \\ +3\gamma_{SO}\delta S_0^4+g_{CO}S_{AI}(s) \end{bmatrix} \tag{11}$$

For the drone search and rescue mission, it is essential to ensure that the temperature distribution of the target and its surrounding area accurately reflects the actual situation. This paper further establishes the boundary condition that "the temperature distribution in a sufficiently large area surrounding the drone search and rescue target is constant over time". This boundary condition assumes that the temperature distribution in a larger vicinity of the target does not undergo significant changes over time, indicating that heat transfer within this range has reached a state of equilibrium, or that the external environment has a minimal impact on the temperature within this range. This constant temperature distribution provides a stable reference for the model, making the calculation process simpler and more efficient.

$$S(a,s)=S_\infty,(a,s)\in\Delta_3^2\times(0,s_r) \tag{12}$$

In this equation, S_∞ can be obtained through interpolation. Since heat transfer occurs not only in the horizontal plane but also in the vertical direction, accurately setting the vertical boundary conditions can help us better understand and predict heat transfer and distribution in the vertical direction, thereby enhancing the overall accuracy of the model. The vertical boundary conditions are given by:

$$\frac{\partial S}{\partial v}(a,s)=0 \tag{13}$$

By integrating the above equations and boundary conditions, we have the following thermal physics model for the drone search and rescue target:

$$\begin{cases} \dfrac{\partial S(a,s)}{\partial s}=\beta_0\sum\limits_{u=1}^{3}\dfrac{\partial^2 S(a,s)}{\partial a_u^2},(a,s)\in\Psi_1\times(0,s_r); \\ \dfrac{\partial S(a,s)}{\partial s}=\beta_t\sum\limits_{u=1}^{3}\dfrac{\partial^2 S(a,s)}{\partial a_u^2}, \\ (a,s)\in(\Psi\setminus\Psi_1)\times(0,s_r); \\ S(a,0)=h(a); \\ -\beta_t\dfrac{\partial S(a,s)}{\partial a_3}=w(s)-oS(a,s),(a,s)\in\Lambda_3^1\times(0,s_r) \\ S(a,s)=S_\infty,\ (a,s)\in\Lambda_3^2\times(0,s_r) \\ \dfrac{\partial S}{\partial v}(a,s)=0. \end{cases} \tag{14}$$

3. SOLUTION OF THE TEMPERATURE DISTRIBUTION MODEL FOR DRONE SEARCH AND RESCUE TARGETS

To integrate the multispectral and thermal imaging technologies of drones, the temperature distribution model must consider not only the thermal physical properties of the ground and targets but also their spectral characteristics. In practical applications, parameters such as the thermal diffusivity of the target, burial depth, height, and cross-sectional area are unknown and need to be derived through the model. By studying the temperature distribution $S(a, s)$, we can relate these physical quantities to temperature variations. This means we need to understand and predict the temperature distribution in the target area through analytical and numerical simulation methods. To achieve this, it is first necessary to clarify the basic principles of temperature distribution and the boundary conditions. The heat diffusion equation is the fundamental equation describing the heat conduction process, considering the physical properties of the target area such as thermal conductivity, density, and specific heat capacity. Due to the complexity of the geometric and physical boundary conditions in practical applications, a direct analytical solution is usually infeasible, thus requiring numerical simulation methods.

The ANSYS software provides powerful tools in this regard. As a finite element analysis software that integrates various physical field analysis functions, ANSYS can accurately simulate the heat conduction process. In practical operations, it is necessary to establish a mesh model of the target area, set the initial and boundary conditions, and then discretize the heat diffusion equation using the finite element method. Through iterative calculations, ANSYS can obtain the temperature distribution across the entire solution area. The solution can be accurately obtained using the following equation:

$$S(a,s)=D(\beta_0,\vartheta_1,g,t) \tag{15}$$

4. MULTISPECTRAL TEMPERATURE INVERSION AND MULTI-TEMPORAL DETECTION

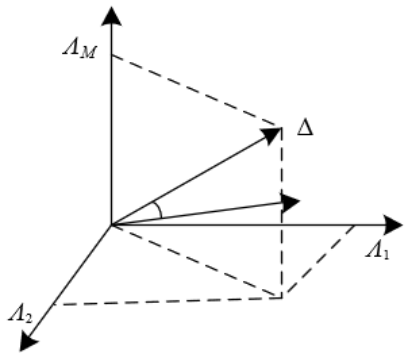

Figure 3. Spectral angle

In drone search and rescue missions, accurately detecting and inverting the temperature distribution in the target area is crucial for locating survivors and assessing environmental conditions. This paper proposes a constrained construction-based multispectral temperature inversion method to improve the accuracy of multispectral temperature inversion in drone SAR tasks. The multispectral infrared imaging system mounted on the drone can capture 48 infrared multispectral simulation images covering the 8-14 μm band. This spectral range encompasses the main infrared spectral features of typical land cover and human radiation, providing rich spectral information. Using this data, the temperature distribution in the target area can be inverted more precisely. According to Planck's law, the radiative capacity of land cover is a function of temperature and wavelength, with different temperatures corresponding to different peak wavelengths of radiation.

Utilizing this characteristic, infrared images in the 8-14 μm band are first obtained through infrared thermal imaging, allowing for an initial inversion of the surface temperature distribution in the area. Next, the radiative spectra of these temperature points are calculated point by point, and the pixel values of the infrared images corresponding to the wavelengths with the highest radiative capacity are selected as the pixel values for the constructed constraint image. The spectral angle of the multispectral vector representing the pixel points is shown in Figure 3. The distribution forms of the spectral angle and the gray information distribution of a specific spectral band are illustrated in Figures 4 and 5.

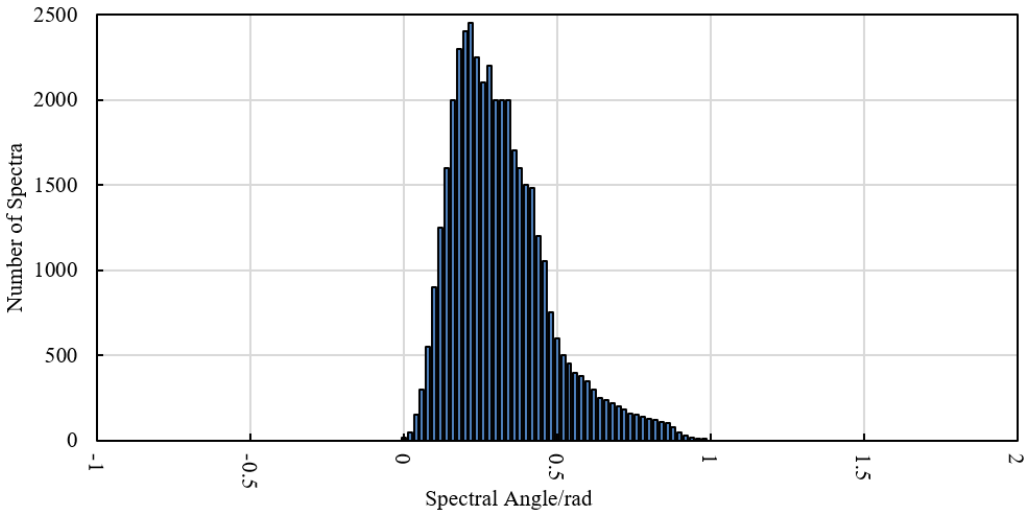

Figure 4. Spectral angle distribution

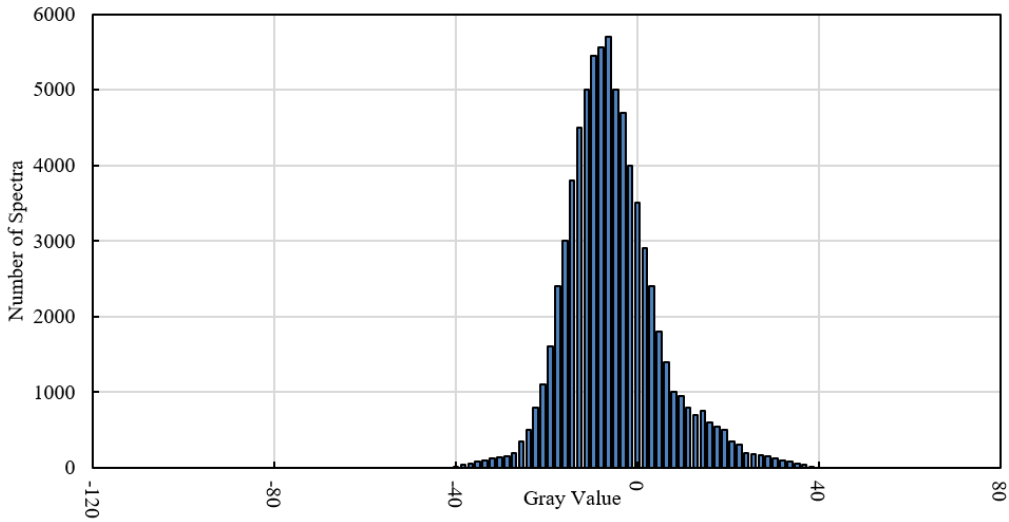

Figure 5. Gray distribution of a single spectral band

After constructing the constraint image, performing temperature inversion based on this image can significantly improve temperature resolution. This is mainly because the selected bands represent the actual radiative capacity more accurately, reducing potential errors and uncertainties in the inversion process. Then, using the temperature data obtained from the inversion, a multispectral temperature inversion result is generated. This result not only provides a higher resolution temperature distribution map but also better highlights the temperature characteristics of humans or other targets, aiding in the accurate localization of rescue targets in complex environments.

By conducting multiple flights and data collections at different time points, drones can capture temperature variations in the target area over time. The accumulation of this multi-temporal data can further correct and validate the temperature inversion results, enhancing the accuracy and reliability of the temperature distribution model. For example, temperature variation data collected during the day and night can help distinguish between natural temperature changes and abnormal temperature hotspots, thus more effectively identifying potential rescue targets. Let's assume that the acquired multi-temporal infrared image sequence is represented as $U(s)$. The problem of detecting the drone search and rescue target can be transformed into finding the minimum of the following equation:

$$H = \int_0^{S_r} \int_{\Gamma_3^{-1}} \left(U(s) - S(a_1, a_2, 0, s) \right)^2 da_1 da_2 ds \tag{16}$$

The set of iterative values that minimizes H is denoted as $n^{\rightarrow H}=(\beta^H_0, \vartheta^H_1, g^H, t^H)$, which can be regarded as the parameters to be solved $n^{\rightarrow}=(\beta_0, \vartheta_1, g, t)$.

Establishing the temperature distribution model is fundamental to the entire process. This model must consider the physical properties of the ground, environmental

conditions, and the thermal characteristics of potential targets. Based on actual conditions, initial and boundary conditions must be input, such as environmental temperature, humidity, wind speed, topography, surface material properties, and a set of estimated values for the parameters to be solved, such as the initial temperature distribution of the target and the locations of heat sources. These input conditions can be obtained through field surveys, historical data, and preliminary multispectral thermal imaging data. Further, ANSYS software can be used to solve the model. The solution from ANSYS yields the theoretical surface temperature distribution of the area, which provides a predicted value. This predicted value offers an initial temperature distribution framework, laying the groundwork for subsequent multi-temporal detection and data fusion.

Figure 6 shows the process of drone search and rescue targeting. Then, actual multispectral infrared images taken at different time points are used for temperature inversion. The drone performs multiple flights at different times to obtain multispectral infrared images covering the target area. These images encompass the 8 to 14 μm bands, providing rich spectral information. Through multispectral temperature inversion techniques, the measured surface temperature distribution of the area is obtained. After acquiring both predicted and measured values, a similarity measure calculation is a crucial step. By comparing the predicted values and measured values of the surface temperature distribution in the area, the similarity measure can be computed. To enhance the model's accuracy, the estimated values of the parameters to be solved need to be continuously updated to minimize the objective function. Through this iterative process, the final parameter estimates that minimize the objective function will be found. These parameter estimates will be output as the final detection results, providing precise temperature distribution information for the target area.

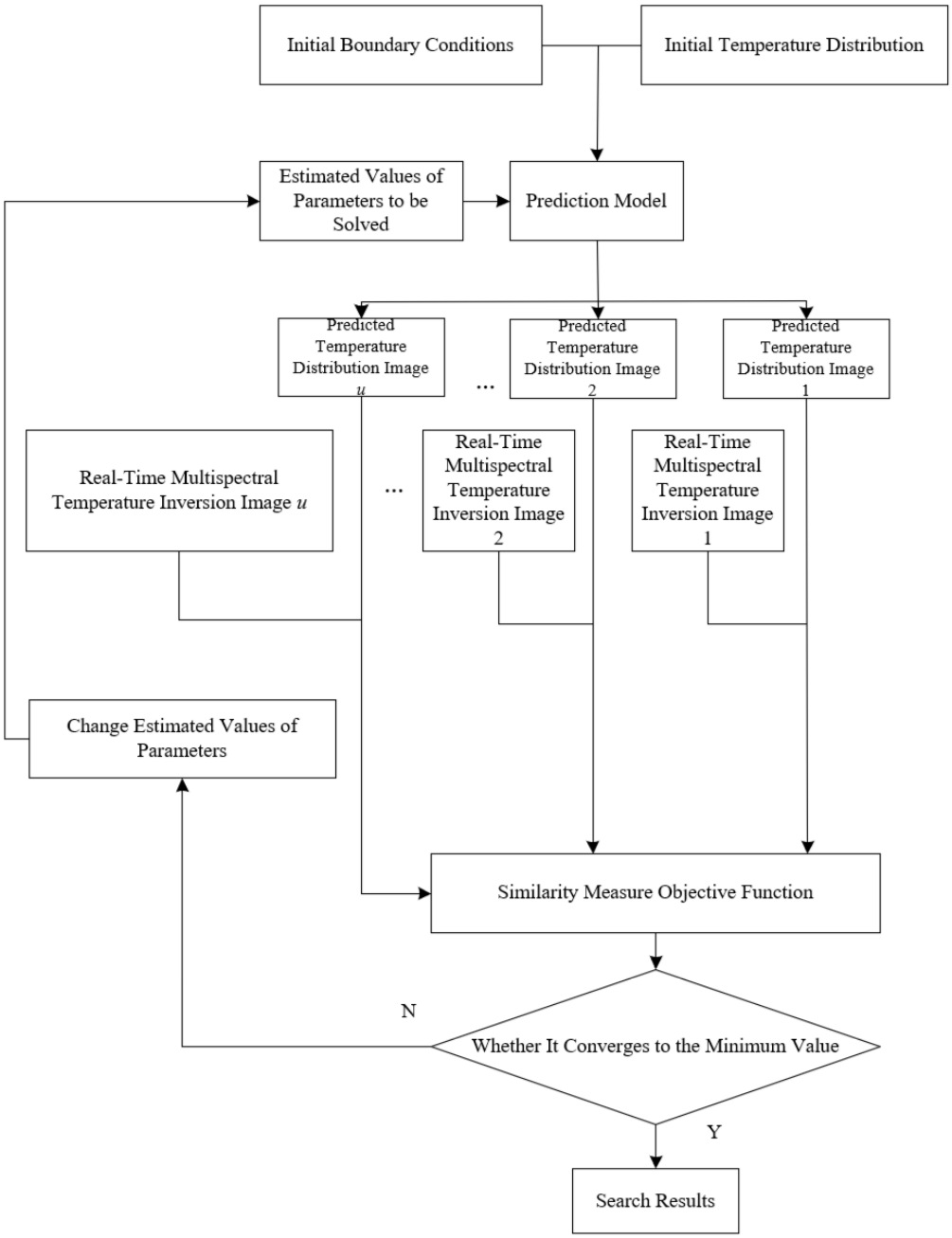

Figure 6. Process of drone search and rescue targeting

5. EXPERIMENTAL RESULTS AND ANALYSIS

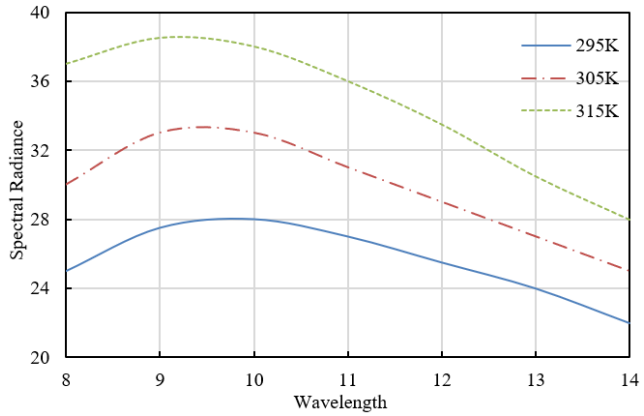

Figure 7. Variation of radiative capability with wavelength at different temperatures (radiation spectrum)

Table 1. Accuracy and loss values of training and testing sets

Model	Learning Rate	Loss Value		Accuracy/%	
		Training Set	Test Set	Training Set	Test Set
The Proposed Model	0.001	0.1789	0.5874	93.51	75
YOLO	0.001	0.1895	0.8123	92.58	73
Mask R-CNN	0.001	0.2563	0.8265	91.37	71

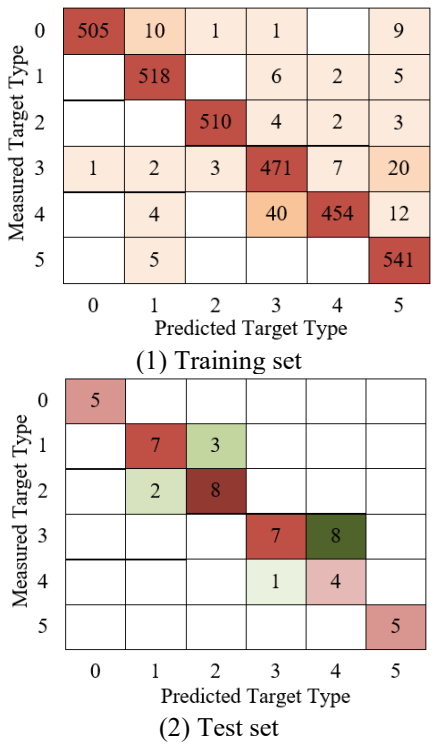

Figure 8. Confusion matrix of training and test sets

In this study, we analyzed the radiation spectra of the target's radiative capabilities at different temperatures (295K, 305K, 315K) as shown in Figure 7. The data indicate that as the temperature increases from 295K to 315K, the radiative capability at all wavelengths significantly increases. For example, at a wavelength of 8 μm, the radiative capabilities are 25 (295K), 30 (305K), and 37 (315K). This trend aligns with the theory of thermal radiation, which states that higher temperatures lead to stronger radiation capabilities. The trend of radiative capability with wavelength is generally similar at different temperatures, displaying an initial increase followed by a decrease. Within the wavelength range of 8 μm to 10 μm, the radiative capability gradually increases, reaching a peak before declining as the wavelength continues to increase. This phenomenon can be attributed to the combined effects of the atmospheric window effect and the thermal radiation characteristics of the target object. Despite the temperature differences, the peak radiation capabilities occur near the wavelengths of 9 μm and 10 μm. Specifically, at 295K and 305K, the peaks are 28 and 33, while at 315K, the peak slightly shifts to 38.5 (at 9 μm). This indicates that the 9 μm to 10 μm band is where the target's radiative capability is strongest and is one of the optimal bands for multispectral temperature inversion. The study demonstrates that establishing a temperature distribution model can more accurately describe the temperature variation characteristics of the target under different environmental conditions. This is crucial for enhancing the precision of multispectral temperature inversions. For instance, through model calibration, we can reduce the environmental interference on radiation measurements, leading to a more accurate inversion of the target's true temperature. Additionally, combining multispectral data from different time points can further improve detection reliability and stability. In complex environments, the temperature changes of the target may be influenced by various factors, and multi-temporal detection can effectively compensate for the limitations of single-time-point detection, providing more comprehensive and accurate temperature distribution information.

From Table 1, we can see that the proposed model has the lowest training loss value of 0.1789, followed by the YOLO model at 0.1895, and the Mask R-CNN model with the highest loss value of 0.2563. A lower loss value generally indicates better fitting capabilities on the training set. The testing loss value of the proposed model is 0.5874, significantly lower than that of the YOLO model (0.8123) and the Mask R-CNN model (0.8265). A lower testing loss value usually suggests stronger generalization ability on unseen data. The training accuracy of the proposed model is the highest at 93.51%, while the YOLO model has an accuracy of 92.58%, and the Mask R-CNN model has the lowest at 91.37%. This further confirms that the proposed model outperforms the other two models on the training set. The testing accuracy of the proposed model is 75%, higher than YOLO's 73% and Mask R-CNN's 71%. A higher testing accuracy indicates better performance on new data. A detailed analysis of the data in Table 1 leads to the following conclusions: The proposed model exhibits the lowest loss values on both the training and testing sets, demonstrating superior fitting capabilities on training data and generalization abilities on new data. The low training loss (0.1789) and low testing loss (0.5874) suggest that the proposed model can effectively handle unseen data. The training accuracy of 93.51% and testing accuracy of 75% are both higher than those of the YOLO and Mask R-CNN models. This indicates that the proposed model offers higher precision in target identification and localization, particularly excelling in applications related to multispectral temperature inversion and multi-temporal detection. The performance of the proposed model on the testing set outperforms that of YOLO and Mask R-CNN, demonstrating better generalization ability. This means that in practical applications, the proposed model can more accurately identify and locate rescue targets,

maintaining reliable detection performance and stability even under complex environmental conditions.

This study enhances the accuracy and reliability of multispectral temperature inversion and multi-temporal detection by establishing and solving a temperature distribution model for drone search and rescue targets, supported by detailed experimental validation. To assess the model's performance, we classified thermal infrared images captured during the drone search and rescue process across different target types. The experimental procedure involved modifying the output of the final fully connected layer of the model to classify five target categories, training the dataset sufficiently while ensuring no overfitting occurred. Confusion matrices for both the training set and test set were generated, as shown in Figure 8, to evaluate the classification performance of the model. The confusion matrix indicates that the model achieved very high classification accuracy for all target types in the training set, with nearly all targets being correctly classified. This suggests that the model has effectively learned the features of various target types during training.

Table 2. Classification performance of the training set

	The Proposed Model			***YOLO***			***Mask R-CNN***		
Target type	Precision %	Recall %	F1-value	Precision %	Recall %	F1-value	Precision %	Recall %	F1-value
0	98.89	98.52	97.85	98.52	97.58	97.58	98.54	95.26	96.25
1	98.23	95.26	97.54	98.62	93.21	96.21	95.26	96.32	95.48
2	96.25	98.26	93.26	95.14	98.54	96.32	98.62	97.25	97.26
3	95.25	93.69	94.51	92.31	92.31	94.52	96.32	92.31	92.32
4	96.54	96.51	95.26	93.25	94.26	94.26	96.15	88.26	92.15
5	98.98	96.54	97.58	96.58	96.23	96.25	92.31	98.62	94.56

Table 3. Classification performance of the test set

	The Proposed Model			***YOLO***			***Mask R-CNN***		
Level	Precision %	Recall %	F1-value	Precision %	Recall %	F1-value	Precision %	Recall %	F1-value
0	100	100	100	92	80	67	100	100	100
1	84.26	61	71.25	63.21	41	74	76.26	71	72.23
2	83.21	91	74	72.26	51	57.56	71.24	81	75.26
3	100	52.32	68.23	98	52.31	68.26	88.56	45.26	61.25
4	44.25	100	61.25	51	93	65.23	32.32	81	48.26
5	102	100	100	82.36	94	91.23	90	100	91

In drone search and rescue missions, the targets were classified into five categories: 0 - Missing Person Rescue, 1 - Disaster Emergency Response, 2 - Maritime Rescue, 3 - Wildlife Conservation and Monitoring, 4 - Infrastructure Monitoring, and 5 - Accident Rescue. Table 2 presents the classification performance of the proposed model, YOLO, and Mask R-CNN on the training set, including precision, recall, and F1 scores across the six target types (0 to 5). For target type 0 (Missing Person Rescue), the proposed model achieved a precision of 98.89%, a recall of 98.52%, and an F1 score of 97.85, outperforming both YOLO (F1 score of 97.58) and Mask R-CNN (F1 score of 96.25). In target type 1 (Disaster Emergency Response), the proposed model again excelled, with a precision of 98.23%, recall of 95.26%, and F1 score of 97.54, compared to YOLO and Mask R-CNN, whose F1 scores were 96.21 and 95.48, respectively, indicating stronger identification and localization capabilities. For target type 2 (Maritime Rescue), while the proposed model had a slightly higher recall, Mask R-CNN performed better overall, achieving an F1 score of 97.26 compared to the proposed model's 93.26. In target type 3 (Wildlife Conservation and Monitoring), YOLO had a slightly higher F1 score of 94.52, although the proposed model had superior precision and recall. For target type 4 (Infrastructure Monitoring), the proposed model outperformed all others on every metric, achieving an F1 score of 95.26, indicating its exceptional performance in this task. Lastly, for target type 5 (Accident Rescue), the proposed model excelled in precision and F1 score, reaching 98.98% and 97.58, respectively, significantly surpassing YOLO and Mask R-CNN.

From Table 3, it is evident that there are significant performance differences among the proposed model, YOLO, and Mask R-CNN across different categories. In level 1 (Disaster Emergency Response) and level 2 (Maritime Rescue), the performance of the proposed model, while lower than levels 0 and 5, still outperformed both YOLO and Mask R-CNN. Specifically, for level 1, the proposed model achieved a precision of 84.26%, recall of 61%, and F1 score of 71.25, which is significantly higher than YOLO's precision of 63.21%, recall of 41%, and F1 score of 74, as well as Mask R-CNN's precision of 76.26%, recall of 71%, and F1 score of 72.23. In level 2, the proposed model also performed well, with a recall of 91%, despite a slightly lower precision. Its F1 score of 74 remains superior to YOLO's 57.56 and Mask R-CNN's 75.26. For level 3 (Wildlife Conservation and Monitoring), the proposed model achieved a precision of 100% with a recall of 52.32% and an F1 score of 68.23, which closely matches YOLO's performance (precision of 98%, recall of 52.31%, F1 score of 68.26) but outperforms Mask R-CNN (precision of 88.56%, recall of 45.26%, F1 score of 61.25). While the recall rate is relatively low, the high precision indicates a tendency for false positives, yet the model effectively identifies targets accurately. In level 4 (Infrastructure Monitoring), the proposed model achieved a recall of 100%, but its precision was only 44.25%, leading to an F1 score of 61.25. While the high recall indicates good coverage, the low precision suggests a high false positive rate. Nonetheless, the proposed model's F1 score still exceeds YOLO's 65.23 (precision of 51%, recall of 93%) and Mask R-CNN's 48.26 (precision of 32.32%, recall of 81%).

Overall, the proposed model demonstrated superior overall performance across categories compared to YOLO and Mask R-CNN, especially excelling in critical tasks such as missing person rescues and accident rescues. Moreover, this research

improved the accuracy of target recognition and localization by establishing and solving a temperature distribution model for drone search and rescue targets, enhancing the precision and reliability of multispectral temperature inversion and multi-temporal detection. Despite some categories showing higher false positive rates, the proposed model significantly improved detection performance and stability in complex environments.

6. CONCLUSION

This study addressed the shortcomings in target recognition and localization during drone search and rescue operations. The research improvements are focused on three key aspects: (1) Establishment of a Temperature Distribution Model: A temperature distribution model for drone search and rescue targets was developed to accurately describe how target temperatures change under various environmental conditions. (2) Mathematical and Physical Solutions: The temperature distribution model was proposed and solved using precise mathematical and physical methods, enhancing the accuracy of target recognition and localization. (3) Multispectral Temperature Inversion and Multi-Temporal Detection: The study explored multispectral temperature inversion and multi-temporal detection techniques, improving the system's detection performance and stability in complex environments. By establishing and solving the temperature distribution model for drone search and rescue targets, this research significantly enhanced the precision and reliability of multispectral temperature inversion and multi-temporal detection. Experimental results indicate that the proposed model demonstrates remarkable detection performance and stability in complex environments, particularly in critical rescue tasks. This study not only introduced new methods and models theoretically but also showcases significant potential in practical applications, providing a solid technological foundation for improving the effectiveness and reliability of drone search and rescue missions.

Despite these notable achievements, some limitations remain. The complexity of the temperature distribution model and its solution process may require substantial computational resources and time, potentially limiting practical applications. While the model considers various environmental conditions, the complexity and variability of real-world environments may still affect its accuracy, necessitating further optimization and adjustment. The model's performance heavily relies on the quality and diversity of training data, requiring a large amount of high-quality annotated data for effective training and validation.

Future research can delve into several areas for further advancement: (1) Optimization of the Temperature Distribution Model and Algorithms: Enhancing computational efficiency to reduce resource consumption. (2) Integration of Diverse Data Types: Performing multi-source data fusion to improve model robustness and adaptability. (3) Real-Time Application Performance: Investigating the model's performance in real-time applications and developing efficient algorithms for real-time processing to enhance drone system responsiveness. (4) Expansion to Broader Applications: Applying the research findings to additional scenarios, such as natural disaster monitoring and environmental protection, to broaden the model's applicability and impact.

In summary, this study employed innovative methods and models to significantly improve target recognition and localization capabilities in drone search and rescue tasks, holding substantial theoretical significance and practical value. Future research will continue to advance the development and application of this field.

REFERENCES

[1] Kumar, G., Anwar, A., Dikshit, A., Poddar, A., Soni, U., Song, W.K. (2022). Obstacle avoidance for a swarm of unmanned aerial vehicles operating on particle swarm optimization: A swarm intelligence approach for search and rescue missions. Journal of the Brazilian Society of Mechanical Sciences and Engineering, 44(2): 56. https://doi.org/10.1007/s40430-022-03362-9

[2] Yang, T., Jiang, Z., Sun, R., Cheng, N., Feng, H. (2020). Maritime search and rescue based on group mobile computing for unmanned aerial vehicles and unmanned surface vehicles. IEEE Transactions on Industrial Informatics, 16(12): 7700-7708. https://doi.org/10.1109/TII.2020.2974047

[3] Shi, X.M. (2022). Thermal environment effect of landscape ecological pattern and dynamic analysis of pattern evolution. International Journal of Heat and Technology, 40(6): 1485-1491. https://doi.org/10.18280/ijht.400617

[4] Wang, Y., Liu, W., Liu, J., Sun, C. (2023). Cooperative USV–UAV marine search and rescue with visual navigation and reinforcement learning-based control. ISA Transactions, 137: 222-235. https://doi.org/10.1016/j.isatra.2023.01.007

[5] Pedersen, C.B., Nielsen, K.G., Rosenkrands, K., Vasegaard, A.E., Nielsen, P., El Yafrani, M. (2021). A grasp-based approach for planning UAV-assisted search and rescue missions. Sensors, 22(1): 275. https://doi.org/10.3390/s22010275

[6] Li, J., Zhang, G., Jiang, C., Zhang, W. (2023). A survey of maritime unmanned search system: Theory, applications and future directions. Ocean Engineering, 285: 115359. https://doi.org/10.1016/j.oceaneng.2023.115359

[7] Kyriakakis, N.A., Marinaki, M., Matsatsinis, N., Marinakis, Y. (2022). A cumulative unmanned aerial vehicle routing problem approach for humanitarian coverage path planning. European Journal of Operational Research, 300(3): 992-1004. https://doi.org/10.1016/j.ejor.2021.09.008

[8] Cao, Y., Qi, F., Jing, Y., Zhu, M., Lei, T., Li, Z., Lu, G. (2022). Mission chain driven unmanned aerial vehicle swarms cooperation for the search and rescue of outdoor injured human targets. Drones, 6(6): 138. https://doi.org/10.3390/drones6060138

[9] García-Moreno, L.M., Díaz-Paz, J.P., Loaiza-Correa, H., Restrepo-Girón, A.D. (2020). Dataset of thermal and visible aerial images for multi-modal and multi-spectral image registration and fusion. Data in Brief, 29: 105326. https://doi.org/10.1016/j.dib.2020.105326

[10] Adamopoulos, E., Rinaudo, F. (2020). UAS-based archaeological remote sensing: Review, meta-analysis and state-of-the-art. Drones, 4(3): 46. https://doi.org/10.3390/drones4030046

[11] Nooralishahi, P., López, F., Maldague, X.P. (2022). Drone-enabled multimodal platform for inspection of

industrial components. IEEE Access, 10: 41429-41443. https://doi.org/10.1109/ACCESS.2022.3167393
[12] Piccinelli, N., De Rossi, G., Daffara, C., Muradore, R. (2024). A passive stereo calibration technique for visible-thermal, low-resolution imaging in remote sensing applications. Measurement, 231: 114647. https://doi.org/10.1016/j.measurement.2024.114647
[13] Kim, D., Lee, J., Quek, T.Q. (2019). Multi-layer unmanned aerial vehicle networks: Modeling and performance analysis. IEEE Transactions on Wireless Communications, 19(1): 325-339. https://doi.org/10.1109/TWC.2019.2944378
[14] Abichandani, P., Lobo, D., Ford, G., Bucci, D., Kam, M. (2020). Wind measurement and simulation techniques in multi-rotor small unmanned aerial vehicles. IEEE Access, 8: 54910-54927. https://doi.org/10.1109/ACCESS.2020.2977693
[15] Wang, G., Song, Y., Liu, C., Yin, Z., Fu, Y., Liang, H. (2024). Spectral efficient two-stage beamforming for UAV MIMO under energy constraint: A budgeted combinatorial MAB-based approach. IEEE Communications Letters, 28(8): 1904-1908. https://doi.org/10.1109/LCOMM.2024.3411097
[16] Roslim, M.H.M., Juraimi, A.S., Che'Ya, N.N., Sulaiman, N., Manaf, M.N.H.A., Ramli, Z., Motmainna, M. (2021). Using remote sensing and an unmanned aerial system for weed management in agricultural crops: A review. Agronomy, 11(9): 1809. https://doi.org/10.3390/agronomy11091809
[17] Hartling, S., Sagan, V., Maimaitijiang, M. (2021). Urban tree species classification using UAV-based multi-sensor data fusion and machine learning. GIScience & Remote Sensing, 58(8): 1250-1275. https://doi.org/10.1080/15481603.2021.1974275
[18] Liu, Y., Liu, G., Sun, H., An, L., Zhao, R., Liu, M., Zhao, F. (2024). Exploring multi-features in UAV based optical and thermal infrared images to estimate disease severity of wheat powdery mildew. Computers and Electronics in Agriculture, 225: 109285. https://doi.org/10.1016/j.compag.2024.109285
[19] Maimaitijiang, M., Sagan, V., Sidike, P., Hartling, S., Esposito, F., Fritschi, F.B. (2020). Soybean yield prediction from UAV using multimodal data fusion and deep learning. Remote sensing of environment, 237: 111599. https://doi.org/10.1016/j.rse.2019.111599
[20] Henn, K.A., Peduzzi, A. (2024). Surface heat monitoring with high-resolution UAV thermal imaging: Assessing accuracy and applications in urban environments. Remote Sensing, 16(5): 930. https://doi.org/10.3390/rs16050930
[21] Zhao, Z., Wang, C., Li, C., Zhang, Y., Tang, J. (2024). Modality conversion meets super-resolution: A collaborative framework for high-resolution thermal UAV image generation. IEEE Transactions on Geoscience and Remote Sensing, 62: 3354878. https://doi.org/10.1109/TGRS.2024.3354878